Spatial-frequency selection of complex degree of coherence of laser images of blood plasma in diagnostics and differentiation of pathological states of human organism of various nosology

A. G. Ushenko,[1,*] P. O. Angelsky,[1] M. Sidor,[1] Yu. F. Marchuk,[2]
D. R. Andreychuk,[2] and N. V. Pashkovskaya[2]

[1]Optics and Publishing Department, Chernivtsi National University, 2 Kotsyubinsky str., Chernivtsi, Ukraine

[2]Clinical Immunology, Allergology and Endocrinology Department, Bucovinian State Medical University,
2 Theatral Sq, Chernivtsi, 58002, Ukraine

*Corresponding author: o.ushenko@chnu.edu.ua

The theoretical background of correlation and phase analysis of laser images of human blood plasma with the spatial-frequency selection of the manifestations of mechanisms of linear and circular birefringence of albumin and globulin is presented. The comparative results of measuring the coordinate distributions of the module of complex degree of coherence (CDC) of laser images of blood plasma taken from the patients of three groups—healthy patients (donors), the patients suffering from the rheumatoid arthritis, and those with stomach cancer (adenocarcinoma)—are shown. The values and ranges of change of the statistical (moments of the 1st–4th order), correlation (excess of autocorrelation functions), and fractal (slopes of approximating curves and dispersion of the extremes of logarithmic dependencies of power spectra) parameters of CDC coordinate distributions are studied. The objective criteria of diagnostics of the pathology and differentiation of the inflammation and oncological state are determined.   © 2014 Optical Society of America

OCIS codes: (260.5430) Polarization; (070.0070) Fourier optics and signal processing; (170.0110) Imaging systems; (170.3880) Medical and biological imaging.

http://dx.doi.org/10.1364/AO.53.00000B

1. Introduction

Among the versatile directions in optical diagnostics of biological objects [1–12], a separate approach of laser polarimetry of polarization azimuth and ellipticity distributions of the images of polycrystalline structures of human tissues and fluids has been differentiated [13–17]. The novel "two-point" analysis of polarization structure of such fields has generalized such an approach. This approach, suggested and developed in a number of theoretical [18–21] and applied [22–24] researches, is based on the use of new correlation parameters for description of interconnections between the coordinate structures of optically anisotropic protein networks [complex degree of mutual anisotropy (CDMA)] and their laser images [complex degree of mutual polarization (CDMP) and complex degree of coherence (CDC)]. Nevertheless, the theoretical basis of polarization correlometry currently applied, which is based on the approximation of only the linear birefringence of optically anisotropic biological layers, requires further development and profound investigation. In

the development of new techniques, it is most important to consider other mechanisms of transformation of parameters of laser radiation—optical activity or circular birefringence, dichroism, etc.

This research is focused on the development and testing the "two-point" method of Fourier polarimetry of CDC of laser images of blood plasma for diagnosing the inflammatory and oncological changes of human organs.

2. Model Presentation

The analysis of forming the field of laser radiation transformed by blood plasma is based on the model of optically anisotropic networks of albumin and globulin suggested in [13–15]. In this research, we shall consider a more general case of generalized optical anisotropy of linear and circular birefringence of protein crystals of the following types:

• Large-scale (the range of linear sizes $l \sim 50 \; \mu m \div 200 \; \mu m$) cylinder-like crystals of albumin with linear birefringence.
• Spherulitic crystals of globulin ($l \sim 5 \; \mu m \div 25 \; \mu m$) with circular birefringence.

The polarization properties of albumin-globulin network of blood plasma are characterized by the generalized matrix of optical anisotropy {D}:

$$\{D\} = \{Q\}\{A\}, \tag{1}$$

where {Q} is the Jones matrix of linear birefringence, and {A} is the Jones matrix of circular birefringence [25]:

$$\{Q\}$$
$$= \left\| \begin{matrix} [\sin^2\rho + \cos^2\rho \exp(-i\delta)] & [\sin\rho \cos\rho(1-\exp(-i\delta))] \\ [\sin\rho \cos\rho(1-\exp(-i\delta))] & [\cos^2\rho + \sin^2\rho \exp(-i\delta)] \end{matrix} \right\|; \tag{2}$$

$$\{A\} = \left\| \begin{matrix} \cos\theta & \sin\theta \\ \sin\theta & \cos\theta \end{matrix} \right\|, \tag{3}$$

Here ρ is the optical axis direction, $\delta = (2\pi/\lambda)\Delta nl$ is the value of phase shift between the orthogonal components of the amplitude of a laser wave with the length λ, which has passed the geometrical path l through the crystal of albumin with linear birefringence Δn, and θ is the rotation angle of the polarization plane of a laser wave caused by optical activity of the substance of globulin crystal.

Taking into account the small value of birefringence $\Delta n \sim 10^{-3}$ and insufficient cross sizes ($d \sim 5 \; \mu m \div 10 \; \mu m$) of protein crystals, we shall further confine ourselves to approximation of weak anisotropy (without affecting the completeness of the analysis), according to which the value and fluctuations of parameters δ and θ are small enough. In this situation, it can be assumed that $\cos(^\delta_\Theta) \approx 1$;

$\sin(^\delta_\Theta) \approx (^\delta_\Theta)$, and the matrix elements in Eqs. (2) and (3) are rewritten in the following way:

$$\{Q\} = \left\| \begin{matrix} [\sin^2\rho + \cos^2\rho(1-i\delta)] & [i\delta \sin\rho \cos\rho.] \\ [i\delta \sin\rho \cos\rho.] & [\cos^2\rho + \sin^2\rho(1-i\delta)] \end{matrix} \right\|; \tag{4}$$

$$\{A\} = \left\| \begin{matrix} 1 & \theta \\ \theta & 1 \end{matrix} \right\|. \tag{5}$$

3. Concise Theoretical Basics of the Method

The "two-point" correlation-phase method of investigation of blood plasma is based on the concept of CDC [20]. This parameter $\mu(r_1, r_2)$ characterizes the correlation between the orthogonal components of the amplitude (E_x, E_y) of laser field in two points with the coordinates r_1 and r_2:

$$\mu(r_1, r_2) = \left[\frac{\text{Tr}(W^\diamond(r_1, r_2)W(r_1, r_2))}{\text{Tr}W(r_1, r_1) \cdot \text{Tr}\, W(r_2, r_2)} \right]. \tag{6}$$

Here $W(r_1, r_2)$ is the transverse spectral density matrix of the following type:

$$W(r_1, r_2) = \begin{bmatrix} E_x^*(r_1)E_x(r_2) & E_x^*(r_1)E_y(r_2) \\ E_y^*(r_1)E_x(r_2) & E_y^*(r_1)E_y(r_2) \end{bmatrix}, \tag{7}$$

where $W^\diamond(r_1, r_2)$ is the Hermitian conjugate matrix to $W(r_1, r_2)$, and Tr is the matrix trace.

Let us write the expression in Eq. (6) for the laser field transformed by the protein crystal [relations in Eqs. (4) and (5)] in its two random points.

In this case, the transverse spectral matrix [relation in Eq. (7)] of density of such a field takes the following form:

$$W_{\text{out}}(r_1, r_2) = D^\diamond(r_1) \cdot W_{\text{in}}(r_1, r_2) \cdot D(r_2). \tag{8}$$

Here $D(r_1)$ and $D(r_2)$ are the Jones matrices of the crystal in the points r_1 and r_2, and $W_{\text{in}}(x_1, x_2)$ is the transverse spectral matrix of density of the probing laser beam:

$$W_{\text{in}}(r_1, r_2) = \begin{bmatrix} E_x^*(r_1)E_x(r_2) & E_x^*(r_1)E_y(r_2) \\ E_y^*(r_1)E_x(r_2) & E_y^*(r_1)E_y(r_2) \end{bmatrix}. \tag{9}$$

Let us determine the analytical form of CDC for the case of probing the protein crystal by the polarized laser wave with the azimuth 0° $E_0 = \left(\begin{matrix} E_{0x} \exp(-i\varphi_{0x}) \\ E_{0y} \exp(-i\varphi_{0y}) \end{matrix} \right) \to E_0(0°) = \left(\begin{matrix} 1 \\ 0 \end{matrix} \right)$. The orthogonal components of the amplitude of Jones vector $E = \left(\begin{matrix} E_x \exp(-i\varphi_x) \\ E_y \exp(-i\varphi_y) \end{matrix} \right)$ of the object wave are determined from the following relations:

$$\begin{cases} E_x(0°) = 1 - i\delta \cos\rho(\cos\rho + \theta \sin\rho); \\ E_y(0°) = \theta - i\delta \sin\rho(\cos\rho + \theta \sin\rho). \end{cases} \tag{10}$$

Taking into account Eqs. ([4](#))–([10](#)), the expression for CDC of the points of the laser image of blood plasma takes the form:

$$\mu(r_1, r_2) = \sqrt{\frac{1}{(a + ib)(\cos^2 \Delta\rho_{12} \cos \Delta\theta_{12} + \sin^2 \Delta\rho_{12} \sin \Delta\theta_{12} \exp(-i \cdot 2\Delta\delta_{12}))}}. \tag{11}$$

Here $\Delta\rho_{12} = \rho(r_1) - \rho(r_2)$, $\Delta\delta_{12} = \delta(r_1) - \delta(r_2)$, and $\Delta\theta_{12} = \theta(r_1) - \theta(r_2)$ "difference" orientation and phase parameters of the polycrystalline network in the points with the coordinates r_1 and r_2, $a + ib$ is the proportionality coefficient.

The analysis of the expression in Eq. ([11](#)) reveals the simultaneous dependence of the CDC value on both the orientation $(\Delta\rho)$ and phase $(\Delta\delta, \Delta\theta)$ structure of polycrystalline network of blood plasma proteins. This ambiguity can be eliminated by means of probing by the beam with circular polarization. In this case, the expression in Eq. ([11](#)) is transformed into sole phase dependence:

$$\mu(r_1, r_2) = \sqrt{\frac{1}{(\exp(-i2\Delta\delta_{12}) \sin \Delta\theta_{12} + \cos \Delta\theta_{12})}}. \tag{12}$$

Further we shall limit ourselves to the consideration of the CDC modulus, the value of which can be measured experimentally:

$$|\mu(r_1, r_2)| = (1 + 2\Delta\delta_{12}\Delta\theta_{12})^{-1}. \tag{13}$$

Thus, to determine the value of $|\mu(r_1, r_2)|$, it is necessary to possess information on the difference of phase shifts between the orthogonal components of the amplitudes $E_x(r_1), E_y(r_1)$ and $E_x(r_2), E_y(r_2)$ in the points with the coordinates r_1, r_2, formed by both the linear $\delta(r_1) - \delta(r_2)$ and circular $\theta(r_1) - \theta(r_2)$ birefringence of blood plasma protein crystals. This information can be experimentally obtained by the technique of polarization phase [[23](#),[24](#)]. Here the object $(\{D\})$ is placed between two crossed phase filters—quarter wave plates $(\{\Phi_1\} = \|\begin{smallmatrix} 1 & 0 \\ 0 & i \end{smallmatrix}\|, \{\Phi_2\} = \|\begin{smallmatrix} i & 0 \\ 0 & 1 \end{smallmatrix}\|)$ and polarizers $(\{P_1\} = \|\begin{smallmatrix} 1 & 1 \\ 1 & 1 \end{smallmatrix}\|; \{P_2\} = \|\begin{smallmatrix} 1 & -1 \\ -1 & 1 \end{smallmatrix}\|)$—the transmission planes of which make angles with the axes of the greatest speed $+45°$ and $-45°$. Analytically the process of the mentioned polarization-phase filtration is described by matrix equation

$$E = 0,5\{P_2\}\{\Phi_2\}\{D\}\{\Phi_1\}\{P_1\}E_0. \tag{14}$$

From Eq. ([14](#)), the following expression for intensity of the transmitted radiation is obtained:

$$I = EE^* = (1 - \theta)^2\delta^2. \tag{15}$$

It is obvious that the value of intensity of the points of polarizationally filtered [relation in Eq. ([14](#))] laser image of blood plasma appears to be the functional $I(\delta, \theta)$. Medically the differentiated information concerning the change of concentration of both albumin and globulin is important for diagnostics of appearance and differentiation of the type of pathological process. For "separation" of the components of the linear (δ) and circular (θ) birefringence, we used the method of spatial-frequency Fourier filtration of distributions of complex amplitudes of the field of laser radiation [[26](#)]. Let us consider the method in more detail. The structure of the field in the focal (frequency) plane of the projection objective can be determined by means of the direct Fourier transform:

$$U_x\left(\frac{X}{\lambda f}, \frac{Y}{\lambda f}\right) \equiv U_x(\nu, \mu) = \frac{1}{i\lambda f} \int_{-\infty}^{\infty} \int E_x(x, y)$$
$$\times \exp[-i2\pi(x\nu + y\mu)]dxdy; \tag{16}$$

$$U_y\left(\frac{X}{\lambda f}, \frac{Y}{\lambda f}\right) \equiv U_y(\nu, \mu) = \frac{1}{i\lambda f} \int_{-\infty}^{\infty} \int E_y(x, y)$$
$$\times \exp[-i2\pi(x\nu + y\mu)]dxdy. \tag{17}$$

Here U_x and U_y are the Fourier-images of distributions $E_x(\rho, \delta, \theta)$ and $E_y(\rho, \delta, \theta)$; $\nu = (X/\lambda f)$ and $\mu = (Y/\lambda f)$ are the spatial frequencies; f is the focus distance.

It is obvious from Eqs. ([16](#)) and ([17](#)) that spatial-frequency structure of distribution of complex amplitudes of the field in the focal plane is determined by superposition of the harmonic components $\exp[-i2\pi(x\nu + y\mu)]$ with the corresponding periods of spatial modulation $L(\nu, \mu) = (\lambda f/\sqrt{\nu^2 + \mu^2})$. It can be easily noticed that for large-scale crystals, a more low-frequency modulation $(L(\delta))$ of Fourier images of distribution of the boundary field $E_{x,y}(\delta)$ complex amplitudes is typical, if compared with the similar parameters $(L(\theta))$ for the boundary field $E_{x,y}(\theta)$, formed by the small-scale network of globulin crystals. In other words, due to the difference of the periods of modulation $L(\theta) < L(\delta)$ in the frequency plane, it is possible to realize selection of such components by means of the vignetting [transparent $R(\Delta\nu, \Delta\mu)$ or opaque $R^{-1}(\Delta\nu, \Delta\mu)$] diaphragm:

$$\begin{cases} \hat{U}_\delta(\nu, \mu) = R(\Delta\nu, \Delta\mu)U(\nu, \mu); \\ \hat{U}_\theta(\nu, \mu) = R^{-1}(\Delta\nu, \Delta\mu)U(\nu, \mu). \end{cases} \tag{18}$$

The partial distributions of complex amplitudes $\begin{bmatrix} \hat{E}_x(\delta, x, y) \\ \dot{E}_x(\theta, x, y) \end{bmatrix}$, $\begin{bmatrix} \hat{E}_y(\delta, x, y) \\ \dot{E}_y(\theta, x, y) \end{bmatrix}$ of the boundary field can be restored by optical realization of the reverse Fourier transform:

$$
\begin{cases}
\begin{bmatrix} \hat{E}_x(\delta, x, y) \\ \dot{E}_x(\theta, x, y) \end{bmatrix} = \text{FT}^{-1} \begin{bmatrix} R(\Delta\nu, \Delta\mu)\hat{U}_x(\nu, \mu) \\ R^{-1}(\Delta\nu, \Delta\mu)\dot{U}_x(\nu, \mu) \end{bmatrix}; \\
\begin{bmatrix} \hat{E}_y(\delta, x, y) \\ \dot{E}_y(\theta, x, y) \end{bmatrix} = \text{FT}^{-1} \begin{bmatrix} R(\Delta\nu, \Delta\mu)\hat{U}_y(\nu, \mu) \\ R^{-1}(\Delta\nu, \Delta\mu)\dot{U}_y(\nu, \mu) \end{bmatrix}.
\end{cases}
\tag{19}
$$

Thus the corresponding spatial-frequency filtered distributions of phases of the laser field formed by the mechanisms of the linear and circular birefringence are determined [relations in Eqs. (15) and (19)]:

$$
\delta(x, y) \approx \sqrt{I(R, x, y)};
\tag{20}
$$

$$
\theta(x, y) \approx \sqrt{I(R^{-1}, x, y)}.
\tag{21}
$$

Based on the relations in Eqs. (13) and (20), in Eq. (21) we obtain the expressions for the modulus of CDC of spatial-frequency filtered laser images:

$$
|\mu(\delta, r_1, r_2)| \approx (1 + 2\Delta\delta_{12})^{-1};
\tag{22}
$$

$$
|\mu(\theta, r_1, r_2)| \approx (1 + 2\Delta\theta_{12})^{-1}.
\tag{23}
$$

4. Technique of Investigation and Algorithms of Data Processing

Experimental research of coordinate distributions of CDC was performed in the setup of Fourier polarimeter (Fig. 1).

Illumination of the layers (smears) of blood plasma was performed by the parallel beam ($\varnothing = 10^4$ μm) of He–Ne laser ($\lambda = 0.6328$ μm) 1. The transmission plane of polarizer 4 and the axis of the highest speed of quarter wave plate 5 (achromatic true zero-order wave plate) made the angle of $\Theta = 45°$.

The smears of blood plasma on the optically homogeneous glass 6 were located in the focal area of micro-objective 7 (Nikon CFI Achromat P; the focal distance is 30 mm, numerical aperture is 0.1, magnification is 4×). In the back focal (Fourier) plane the vignetting diaphragm 8 was located [relation in Eq. (18)]. The polarization micro-objective 9 (Nikon CFI Achromat P; the focal distance is 30 mm, numerical aperture is 0.1, magnification is 4×) was superposed with the spatial plane of micro-objective 7 on the focus distance, and the reverse Fourier transform of polarizationally filtered field of laser radiation [relations in Eq. (14)] was realized (relations in Eqs. (19) and (20)]. Coordinate distribution of intensity [relations in Eqs. (15), (21), (22)] of such a field was recorded in the plane of light-sensitive plate of CCD camera 12 ($m \times n = 600$ pix × 800 pix), located at the focus distance from micro-objective 9. CCD camera 12 [the imaging source DMK 41AU02.AS, monochrome 1/2 in. CCD, Sony IC-X205AL (progressive scan), overall amount of pixels is $m \times n = 1280 \times 960$, light sensitive area size is 7600×6200 μm, sensitivity is 0.05 lx, dynamic range is 8 bit, deviation of photosensitive characteristics from linear no more then 12%] provided the range of measurement of structural elements of the reconstructed image of blood plasma layer from 2 to 2000 μm and measured the distributions $I_\delta(m \times n)$ and $I_\theta(m \times n)$. Further, according to Eqs. (21) and (22), the coordinate distributions $\delta(m \times n)$ and $\theta(m \times n)$ were calculated, which were scanned with the step

$$
\begin{pmatrix}
r_{11} & r_{11} + \Delta r & \dots & r_{1m} \\
\downarrow & & & \downarrow \\
\rightarrow & \rightarrow & \rightarrow & \rightarrow \\
\downarrow & & & \downarrow \\
r_{n1} & r_{n1} + \Delta r & \dots & r_{nm}
\end{pmatrix}
$$

$\Delta r = 1$ pix by line. For each pair of points $(r_{ik}, r_{ik} + \Delta r)$ on the basis of relations in Eqs. (23) and (24), the value of CDC modulus, $\mu_\delta(r_{ik}, r_{ik} + \Delta r)$ and $\mu_\theta(r_{ik}, r_{ik} + \Delta r)$, was determined. As a result, the coordinate distributions
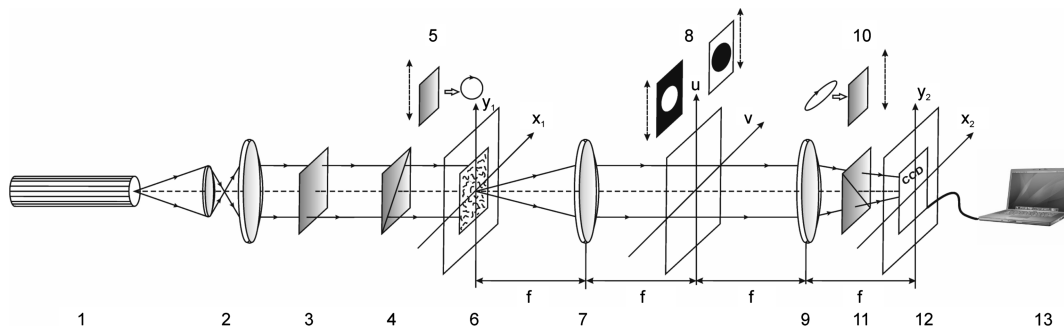
F1:1 Fig. 1. Optical scheme of Fourier polarimeter, where 1, is the He–Ne laser; 2, is the collimator; 3, is the stationary quarter wave plate; 5,
F1:2 10, are the rotating quarter wave plates; 4, 11, are the polarizer and analyzer; 6, is the object of investigation; 7, 9, are the polarization
F1:3 micro-objectives; 8, is the vignetting diaphragm; 12, is the CCD camera; 13, is the computer.

$$\mu_{\delta,\theta}\begin{pmatrix} (r_{11};r_{11}+\Delta r) & \ldots & (r_{1m-1},r_{1m-1}+\Delta r) \\ \ldots & \ldots & \ldots \\ (r_{n1},r_{n1}+\Delta r) & \ldots & (r_{nm-1},r_{nm-1}+\Delta r) \end{pmatrix}$$

of blood plasma images were found. For objective estimation of such distributions, we used the complex statistical, correlation, and fractal analysis.

The ensemble of statistical moments of the 1st and 4th orders $Z^{\mu}_{j=1,2,3,4}$ was calculated based on the following relations [15–17]:

$$Z^{\mu}_1 = \frac{1}{N}\sum_{i=1}^{N}|\mu_i|, \qquad Z^{\mu}_2 = \sqrt{\frac{1}{N}\sum_{i=1}^{N}\mu_i^2},$$

$$Z^{\mu}_3 = \frac{1}{(Z^{\mu}_2)^3}\frac{1}{N}\sum_{i=1}^{N}\mu_i^3, \qquad Z^{\mu}_4 = \frac{1}{(Z^{\mu}_2)^2}\frac{1}{N}\sum_{i=1}^{N}\mu_i^4. \quad (24)$$

Here N is the number of pixels of the CCD camera.

The CDC analysis was grounded on the technique of autocorrelation with the use of the function [15–17]:

$$K^{\mu}_{i=1\div n}(\Delta m) = \lim_{m\to 0}\frac{1}{m}\int_1^m [\mu(m)][\mu(m-\Delta m)]\mathrm{d}m. \quad (25)$$

Here $(\Delta m = 1$ pix$)$ is the "step" with which the coordinates $(x = 1 \div m)$ of CDC distribution for every separate i-th line of CCD camera pixels change.

The resulting expression of autocorrelation function was obtained by averaging the partial functions in Eq. (25) by all the lines of $i = 1 \div n$:

$$K^{\mu}(\Delta m) = \frac{\sum_{i=1}^{n}K^{\mu}_i(\Delta m)}{n}. \quad (26)$$

For the quantitative characteristics of autocorrelation dependencies $K^{\mu}(\Delta m)$, we chose the "correlation moment" Q^{μ}_4, which determines their excess:

$$Q = \frac{\sum_{i=1}^{N}(K(\Delta m))_i^4}{\left(\sum_{i=1}^{N}(K(\Delta m))_i^2\right)^2}. \quad (27)$$

The fractal analysis [15–17] of distributions $\mu(m \times n)$ was grounded on calculation of logarithmic dependencies $\log J(\mu) - \log d^{-1}$ of power spectra $J(\mu)$; where $\nu = d^{-1}$, spatial frequencies determined by geometrical sizes (d) of structural elements of laser images of the blood plasma layer. All the distributions $\log J(\mu) - \log d^{-1}$ were characterized by dispersion

$$D^{\mu} = \sqrt{\frac{1}{N}\sum_{i=1}^{N}[\log J(\mu) - \log d^{-1}]_i^2}. \quad (28)$$

To classify the distributions $\mu(m \times n)$, the dependencies $\log J(\mu) - \log d^{-1}$ were approximated by the least-squares method into curves $V(\eta)$:

- $\mu(m \times n)$ is the fractal or scale-self-similar if there is a constant inclination angle η within two to three decades of d sizes change;
- $\mu(m \times n)$ is the multifractal if there are several angles η;
- $\mu(m \times n)$ is random if there are no stable inclination angles η.

5. Experimental Results and Discussion

As objects of investigation, three groups of optically thin (attenuation coefficient $\tau \approx 0,077 \div 0,084$) layers of blood plasma smears dried at room temperature were taken from the patients with the following diagnoses:

- Group 1 is healthy (donors) people: 23 samples.
- Group 2 is the inflammation process (rheumatoid arthritis): 22 samples.
- Group 3 is cancer (adenocarcinoma of stomach): 19 samples.

To determine the conditions of effective differentiation of manifestations of linear [relations in Eqs. (2) and (4)] and circular [relations in Eqs. (3) and (5)] birefringence of polycrystalline networks of blood plasma, the sizes of the vignetting diaphragm were changed within 10 μm ÷ 200 μm. The size $(R = 50$ μm; $R^{-1} = 30$ μm$)$ at which the ensemble of statistical moments of the 1st–4th orders $Z^{\mu}_{j=1,2,3,4}$ [relations in Eq. (25)] characterizing the CDC distributions $\mu_{\delta,\theta}(x = 1 \div m - 1, y = 1 \div n)$ reach their extreme values was considered optimal.

The diagnostic potentiality of Fourier polarimetry is illustrated by the dependencies presented in Figs. 2–4.

The comparative analysis of histograms [(b), (f), (j)], autocorrelation functions [(c), (g), (k)] and logarithmic dependencies of power spectra [(d), (h), (l)] of distributions $|\mu(r_1, r_2)|$ revealed the sufficient difference between the test group (donors) and Groups 2 and 3. Statistically such dependencies manifest themselves in the transformations of histograms of CDC of laser images of plasma [Fig. 2, fragments (b) and (f), (j)]. It is obvious that for histograms $|\mu(r_1, r_2)|$ of the images of blood plasma taken from healthy people, the localization of the main extreme in the domain of maximal values of CDC is typical. This indicates rather weak phase fluctuations caused by the polycrystalline network of blood plasma proteins [relations in Eqs. (4) and (5)], as the consequence of which [relation in Eq. (13)] $|\mu(r_1, r_2)| \to 1$.

For pathological states (Groups 2 and 3), the increase of birefringence of polycrystalline networks is mainly due to the growth of globulin concentration. Thus the increase of phase modulation leads to the shift of histograms extremes [Fig. 2, fragments (f), (j)] in the domain of smaller values of CDC $(|\mu(r_1, r_2)| \to 0, 5)$. Besides, autocorrelation functions $K^{\mu}(\Delta m)$ of coordinate distributions $\mu(m \times n)$ [Fig. 2, fragments (g), (l)] decrease faster. This fact also proves the increasing phase heterogeneity of laser images of blood plasma of patients with rheumatoid
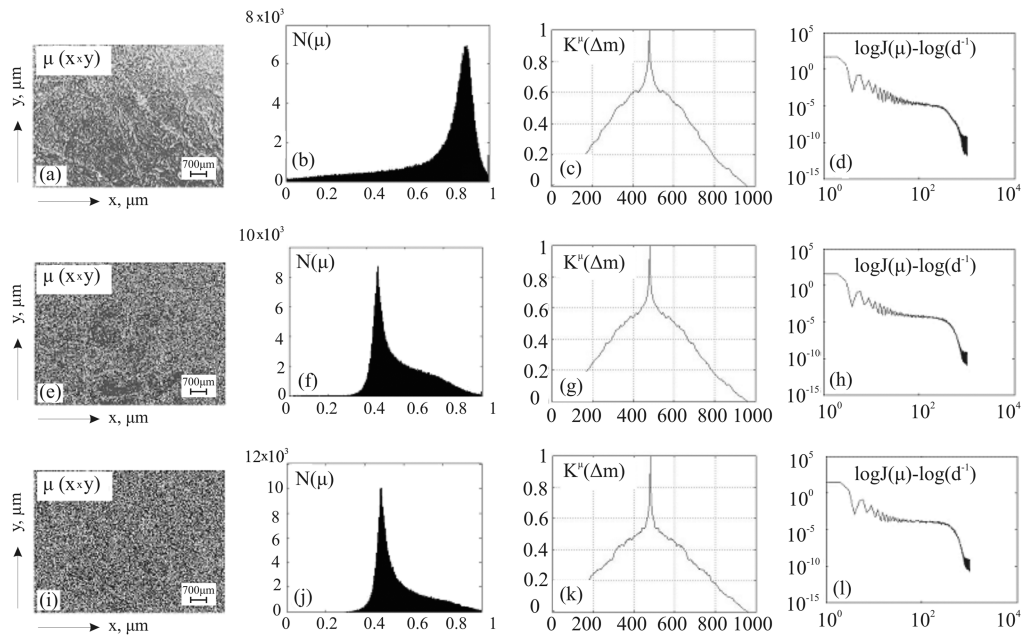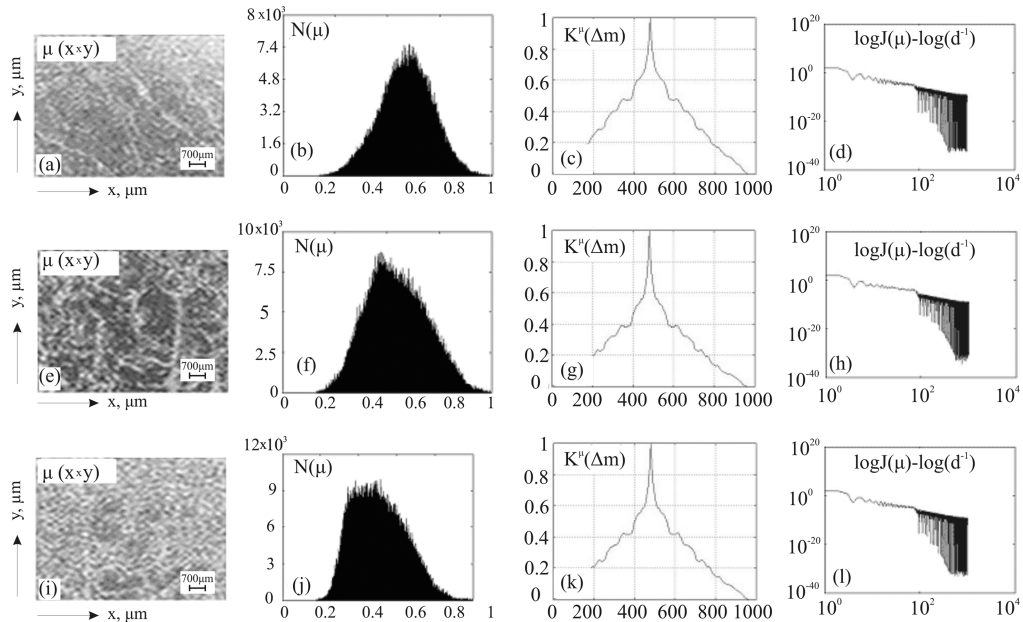
F2:1 Fig. 2. Coordinate structure [(a), (e), (i)], histograms [(b), (f), (j)], autocorrelation functions [(c), (g), (k)], and logarithmic dependencies of
F2:2 power spectra [(d), (h), (l)] of CDC distributions of the images of blood plasma of the patients from Group 1 [(a), (b), (c), (d)], Group 2 [(e), (f),
F2:3 (g), (h)], and Group 3 [(i), (j), (k), (l)].

362 arthritis (Group 2) and patients with stomach
363 cancer (Group 3). In addition, random coordinate
364 distributions $\mu(m \times n)$ are being formed; the range
365 of geometrical sizes of crystals increases in the
366 range, within which there is no stable slope for
367 approximating curves $V(\eta)$ [Fig. 2, fragments (d)
368 and (h), (m)]. Also differentiation of the type and de-
369 gree of pathological state severity {"inflammation
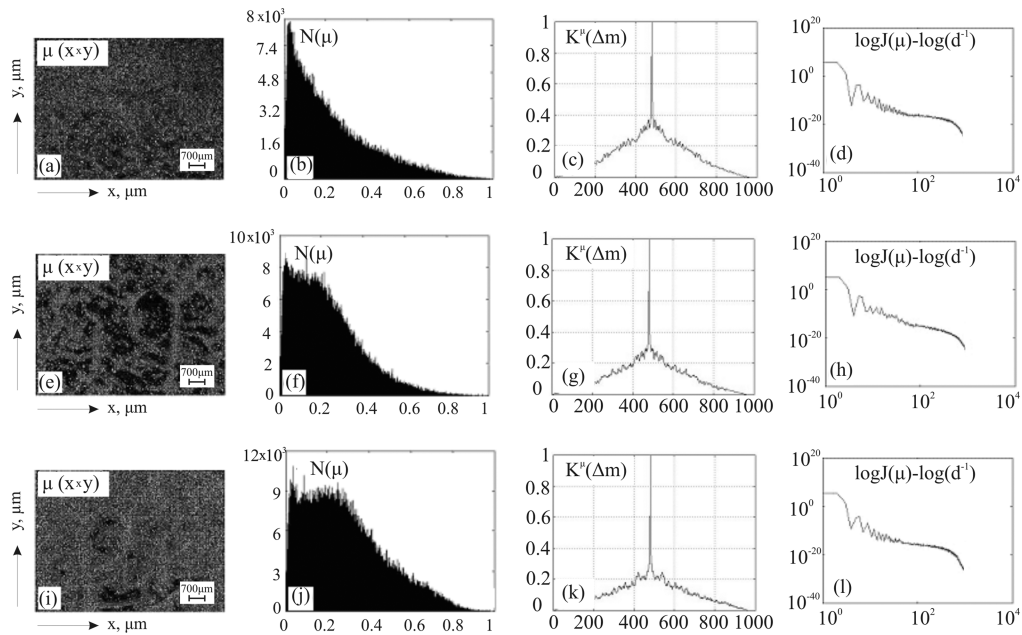370 process [Fig. 2, fragments (e), (f), (g), (h)]; cancer

371 [Fig. 2, fragments (i), (j), (l), (m)]"} is practically
372 impossible (Table 1).
373 The results of the method of spatial-frequency
374 large-scale Fourier selection of polarizationally fil-
375 tered laser images of the samples of all groups are
376 illustrated by the dependencies presented in Fig. 3.
377 The comparative analysis of the set of parameters
378 characterizing the coordinate distributions
379 $|\mu(\delta, r_1, r_2)|$ revealed certain difference between them.

F3:1 Fig. 3. Coordinate structure [(a), (e), (i)], histograms [(b), (f), (j)], autocorrelation functions [(c), (g), (k)], and logarithmic dependencies of
F3:2 power spectra [(d), (h), (l)] of CDC distributions $|\mu(\delta, r_1, r_2)|$ of the points of spatial-frequency filtered laser images of large-scale polycrystal-
F3:3 line network of albumin of blood plasma layers of the patients from Group 1 [(a), (b), (c), (d)], Group 2 [(e), (f), (g), (h)], and Group 3 [(i), (j),
F3:4 (k), (l)].

Namely, the histograms of distribution of CDC values of laser images of blood plasma taken from the patients of Groups 2 and 3 are characterized by the asymmetric form in relation to the main extreme [Fig. 3, fragments (f), (j)] if compared with the similar distribution found for the sample of blood plasma of a healthy donor [Fig. 3, fragment (b)]. The determined peculiarity, in our opinion, is related to some increase of concentration of not only globulin, but also of albumin in the blood of sick patients. As a result of biochemical process, the level of linear birefringence [relations in Eqs. (2) and (4)] and the corresponding phase modulation $\delta(m \times n)$. Therefore, in the histograms $|\mu(\delta, r_1, r_2)|$, small values of CDC are more probable [relation in Eq. (22)]. Moreover, for a more severe pathological process (adenocarcinoma of stomach), the degree of asymmetry increases [Fig. 3, fragments (f) and (j)].

The dependencies of autocorrelation functions of CDC distributions of laser images of the large-scale component of polycrystalline networks of blood plasma albumin smoothly and monotonously

decrease [Fig. 3, фрагменты (c), (g), (l)]. This fact indicates to the coordinately homogeneous structure of the corresponding distributions $|\mu(\delta, r_1, r_2)|$. Besides, the scale-self-similar structure of such distributions was revealed; the logarithmic dependencies of power spectra of distributions $|\mu(\delta, r_1, r_2)|$ are characterized by the same inclination angle in practically all the range of change of geometrical sizes from 2 to 1000 μm [Fig. 3, fragments (d), (h), (l)].

Thus, the "asymmetrization" of histograms of CDC distributions $|\mu(\delta, r_1, r_2)|$ appeared to be the main criterion of differentiation of inflammation and oncological changes in human organisms.

Quite a different situation is observed at the complex statistical, correlation, and fractal analyses of spatial-frequency filtered coordinate distributions of CDC of laser images of small-scale optically active networks of globulin (Fig. 4).

The comparison of the results obtained (Fig. 4) revealed the following polarization-correlation features of appearance of the pathological process. First, it is a sufficient increase of probability of CDC values of laser images of blood plasma of Groups 2 and 3 in the domain of minimal values $0 \leq \mu_\theta \leq 0,35$ [Fig. 4, parts (f) and (j)]. Second, the "pathological" increase of the influence of circular birefringence of polycrystalline network of blood plasma leads to the formation of chaotically located centers of phase modulation. This process is correlationally manifested in a faster fall (decrease of half-width) of the corresponding autocorrelation dependencies [Fig. 4, fragments (i) and (l)]. It should be noted that the above-mentioned features are more obvious for stomach cancer.

Quantitatively the difference between the coordinate distributions of the parameters of CDC of laser

Table 1. Parameters P of Statistical, Correlation, and Self-Similar Structure of Coordinate Distributions of CDC Laser Images of Polycrystalline Networks of Protein Networks of Blood Plasma

P	Group 1	Group 2	Group 3
Z_1	$0,85 \pm 0,13$	$0,44 \pm 0,058$	$0,42 \pm 0,061$
Z_2	$0,16 \pm 0,024$	$0,14 \pm 0,023$	$0,13 \pm 0,021$
Z_3	$2,77 \pm 0,44$	$1,54 \pm 0,26$	$1,41 \pm 0,19$
Z_4	$1,08 \pm 0,15$	$2,21 \pm 0,31$	$2,42 \pm 0,38$
Q_4	$0,24 \pm 0,037$	$1,15 \pm 0,19$	$1,38 \pm 0,23$
$V(\eta)$	Fractal	Random	Random
D	$0,23 \pm 0,032$	$0,26 \pm 0,034$	$0,28 \pm 0,039$

Table 2. Parameters P of Statistical, Correlation and Self-Similar Structure of Coordinate Distributions of CDC of Laser Images of Protein Polycrystalline Networks of Blood Plasma

	μ_δ			μ_θ		
P	Group 1	Group 2	Group 3	Group 1	Group 2	Group 3
Z_1	$0,63 \pm 0,11$	$0,59 \pm 0,091$	$0,55 \pm 0,008$	$0,11 \pm 0,014$	$0,15 \pm 0,028$	$0,25 \pm 0,034$
Z_2	$0,27 \pm 0,045$	$0,25 \pm 0,038$	$0,22 \pm 0,022$	$0,09 \pm 0,013$	$0,14 \pm 0,033$	$0,23 \pm 0,037$
Z_3	$0,07 \pm 0,01$	$0,41 \pm 0,069$	$2,11 \pm 0,37$	$2,23 \pm 0,31$	$1,11 \pm 0,17$	$0,53 \pm 0,12$
Z_4	$0,08 \pm 0,012$	$0,17 \pm 0,031$	$0,22 \pm 0,034$	$1,56 \pm 0,27$	$0,85 \pm 0,12$	$0,41 \pm 0,075$
Q_4	$0,04 \pm 0,007$	$0,05 \pm 0,009$	$0,055 \pm 0,73$	$1,14 \pm 0,19$	$2,45 \pm 0,29$	$4,05 \pm 0,61$
$V(\eta)$	Fractal	Fractal	Fractal	Random	Random	Random
D	$0,32 \pm 0,052$	$0,29 \pm 0,041$	$0,27 \pm 0,037$	$0,14 \pm 0,022$	$0,11 \pm 0,018$	$0,13 \pm 0,016$

images of blood plasma crystals with linear μ_δ and circular μ_θ birefringence is illustrated by the data presented in Table 2.

The comparative analysis of the data obtained revealed the following parameters, effective in diagnostics and differentiation of various pathological states (presented in gray):

• The statistical moment of the 3rd order (Z_3) characterizing the distributions μ_δ of laser images of linearly birefringent crystals of albumin; the intergroup difference lies within 5–6 times.

• The complete set of statistical moments $Z_{i=1;2;3;4}$ of distributions μ_θ of laser images of the network of crystals of globulin with circular birefringence; the range of intergroup difference is 1.5–4 times.

• The correlation moment of the 4th order (Q_4) of autocorrelation functions of distributions μ_θ; the intergroup difference of the values of this parameter lies within the range of 2.1–3.6 times.

6. Conclusions

The method of correlation-phase analysis of laser images of polycrystalline networks of proteins of blood plasma layers with spatial-frequency filtration of manifestations of linear and circular birefringence of albumin and globulin was suggested and analytically substantiated.

The comparative investigation of the effectiveness of the developed method in diagnostics of the appearance and differentiation of the severity degree ("inflammation process; cancer") of pathological state of human organism was performed.

The criteria of rheumatoid arthritis and stomach cancer differentiation on the basis of the statistical, correlation, and fractal analyses of the spatial-frequency filtered CDC distributions of laser images of polycrystalline albumin-globulin networks were determined.

References

1. X. Wang and L.-H. Wang, "Propagation of polarized light in birefringent turbid media: a Monte Carlo study," J. Biomed. Opt. **7**, 279–290 (2002).
2. O. V. Angelsky, A. Y. Bekshaev, P. P. Maksimyak, A. P. Maksimyak, I. Mokhun, S. G. Hanson, C. Y. Zenkova, and A. V. Tyurin, "Circular motion of particles suspended in a Gaussian beam with circular polarization validates the spin part of the internal energy flow," Opt. Express **20**, 11351–11356 (2012).
3. V. V. Tuchin, *Tissue Optics: Light Scattering Methods and Instruments for Medical Diagnosis*, 2nd ed. (SPIE Press, 2007), PM 166.
4. A. Y. Bekshaev, O. V. Angelsky, S. G. Hanson, and C. Y. Zenkova, "Scattering of inhomogeneous circularly polarized optical field and mechanical manifestation of the internal energy flows," Phys. Rev. A **86**, 023847 (2012).
5. A. Yu. Seteikin, "Monte Carlo analysis of the propagation of laser radiation in multilayer biomaterials," Russ. Phys. J. **48**, 280–284 (2005).
6. J. F. de Boer, T. E. Milner, M. G. Ducros, S. M. Srinivas, and J. S. Nelson, *Handbook of Optical Coherence Tomography*, B. E. Bouma and G. J. Tearney, eds. (Marcel Dekker, 2002), pp. 237–274.
7. S. Jiao, M. Todorovic, G. Stoica, and L. V. Wang, "Fiber-based polarization-sensitive Mueller matrix optical coherence tomography with continuous source polarization modulation," Appl. Opt. **44**, 5463–5467 (2005).
8. S. Makita, Y. Yasuno, T. Endo, M. Itoh, and T. Yatagai, "Jones matrix imaging of biological samples using parallel-detecting polarization-sensitive Fourier domain optical coherence tomography," Opt. Rev. **12**, 146–148 (2005).
9. S. Makita, Y. Yasuno, T. Endo, M. Itoh, and T. Yatagai, "Polarization contrast imaging of biological tissues by polarization-sensitive Fourier-domain optical coherence tomography," Appl. Opt. **45**, 1142–1147 (2006).
10. M. C. Pierce, J. Strasswimmer, B. H. Park, B. Cense, and J. F. de Boer, "Birefringence measurements in human skin using polarization-sensitive optical coherence tomography," J. Biomed. Opt. **9**, 287–291 (2004).
11. Y. Yasuno, S. Makita, Y. Sutoh, M. Itoh, and T. Yatagai, "Birefringence imaging of human skin by polarization-sensitive spectral interferometric optical coherence tomography," Opt. Lett. **27**, 1803–1805 (2002).
12. V. V. Tuchin, "A clear vision for laser diagnostics," IEEE J. Select. Topics on Quantum Electronics **13**, 1621–1628 (2007).
13. A. G. Ushenko, "Laser polarimetry of polarization-phase statistical moments of the object field of optically anisotropic scattering layers," Opt. Spectrosc. **91**, 313–316 (2001).
14. O. V. Angel'skiǐ, A. G. Ushenko, A. D. Arkhelyuk, S. B. Ermolenko, and D. N. Burkovets, "Scattering of laser radiation by multifractal biological structures," Opt. Spectrosc. **88**, 444–447 (2000).
15. A. G. Ushenko, "Polarization structure of biospeckles and the depolarization of laser radiation," Opt. Spectrosc. **89**, 597–600 (2000).
16. A. N. Bashkatov, E. A. Genina, and V. V. Tuchin, "Optical properties of skin, subcutaneous, and muscle tissues: a review," J. Innovative Optical Health Sciences **4**, 9–38 (2011).
17. O. V. Angelsky, Yu. Ya. Tomka, A. G. Ushenko, Ye. G. Ushenko, and Yu. A. Ushenko, "Investigation of 2D Mueller matrix structure of biological tissues for preclinical diagnostics of their pathological states," J. Phys. D **38**, 4227–4235 (2005).
18. F. Gori, M. Santarsiero, S. Vicalvi, R. Borghi, and G. Guattari, "Beam coherence-polarization matrix," Pure Appl. Opt. **7**, 941–951 (1998).
19. Wolf, "Unified theory of coherence and polarization of random electromagnetic beams," Phys. Lett. A **312**, 263–267 (2003).

543 20. J. Tervo, T. Setala, and A. Friberg, "Degree of coherence for electromagnetic fields," Opt. Express **11**, 1137–1143 (2003).
545 21. J. Ellis and A. Dogariu, "Complex degree of mutual polarization," Opt. Lett. **29**, 536–538 (2004).
547 [5] 22. O. V. Angel'skii, A. G. Ushenko, A. D. Archelyuk, S. B. Ermolenko, and D. N. Burkovets, "Structure of matrices for the transformation of laser radiation by biofractals," Quantum Electron. **29**, 1074–1077 (1999).
551 23. Y. O. Ushenko, Y. Ya. Tomka, I. Z. Misevitch, V. V. Istratiy, and O. I. Telenga, "Complex degree of mutual anisotropy of biological liquid crystals nets," Opt. Eng. **50**, 039001 (2011).
555 24. Yu. A. Ushenko, Y. Y. Tomka, and A. V. Dubolazov, "Complex degree of mutual anisotropy of extracellular matrix of biological tissues," Opt. Spectrosc. **110**, 814–819 (2011).
559 25. A. Gerrard and J. M. Burch, *Introduction to Matrix Methods in Optics* (Wiley-Interscience, 1975).
561 26. J. W. Goodman, *Laser Speckle and Related Phenomena*, J. C. Dainty ed. (Springer-Verlag, 1975), pp. 9–75.

Queries

1. AU: This sentence does not appear to be complete. What happens as a result?

2. AU/ED: Translate to English?

3. A check of online databases revealed a possible error in this reference. The fpage has been changed from '53' to '280'. Please confirm this is correct.A check of online databases revealed a possible error in this reference.
563   The lpage has been changed from '57' to '284'. Please confirm this is correct.

4. AU: Please add author's first initials for ref. [19].

5. AU: Please check this author name "Angel`skii" is correct for ref. [22].